$Cr_3Si_2O_7 \cdot {}^1/_4MX$ (MX = NaCl, NaBr, KCl, KBr): A Cage Structure Built from $[Cr^{II}O_4]$ and $[Si_2O_7]$ Units[1]

Anita Schmidt and Robert Glaum*,†

Institut für Anorganische und Analytische Chemie der Justus-Liebig-Universität Giessen, Heinrich-Buff-Ring 58, D-35392 Giessen, Germany

Received January 22, 1997[⊗]

The new compounds $Cr_3Si_2O_7 \cdot {}^1/_4MX$ (MX = NaCl, NaBr, KCl, KBr) form a series of chromous disilicates hosting alkali-metal halides in a framework structure. Purple crystals with edge lengths up to 1 mm were prepared by reacting mixtures of Cr_2O_3, Cr, SiO_2, and the respective alkali-metal halide in evacuated silica tubes at ∼1620 K for 2 days. The structures of $Cr_3Si_2O_7 \cdot {}^1/_4NaCl$, $Cr_3Si_2O_7 \cdot {}^1/_4NaBr$, $Cr_3Si_2O_7 \cdot {}^1/_4KCl$ and $Cr_3Si_2O_7 \cdot {}^1/_4KBr$ (*I*4/*mmm* (No. 139), $Z = 8$, $a \sim 10.3$ Å, $c \sim 12.97$ Å) have been solved and refined from X-ray single-crystal data. The framework consists of two crystallographically independent Cr^{II} in square planar oxygen coordination. Three of those squares form a bent trimer $[Cr_3O_4O_{4/2}]$. Four trimers are connected through vertices forming a $[Cr_{12}O_{24}]$ cage wherein the halide ion is sited. By the linking of individual $[Cr_{12}O_{24}]$ units, disilicate groups form a second type of cage which is occupied by Na^+ or K^+. The disilicate groups are in eclipsed conformation with a bridging angle ∠(Si,O1,Si) ∼ 125°. Magnetic measurements indicate strong low-dimensional antiferromagnetic interactions among the Cr^{II} ions. The UV/vis spectrum of $Cr_3Si_2O_7 \cdot {}^1/_4NaBr$ is reported.

Introduction

For chromium(II) oxo compounds a particular stereochemistry, unusual cooperative magnetic behavior and interesting spectroscopic properties can be expected due to the d^4 electron configuration. However, not many compounds containing chromium(II) coordinated by oxygen only or by oxygen and halogen have been synthesized until now. Among the few crystallographically well-characterized compounds of divalent chromium are $Cr_2P_2O_7$,[2,3] $Cr_3(PO_4)_2$,[4] the mixed-valent chromium(II,III) phosphates $Cr_7(PO_4)_6$[5] and $Cr_6(P_2O_7)_4$,[6] the boracites $Cr_3B_7O_{13}X$ (X: Cl, Br, I),[7−9] the silicates $CaCrSi_4O_{10}$[10] and Cr_2SiO_4,[11] and the halide disilicates $Cr_4(Si_2O_7)X_2$ (X = Cl, Br),[12] which we have described recently. In this article we report the synthesis, crystal structure, and properties of a new series of compounds $M(Cr_3Si_2O_7)_4X$ or rather $Cr_3Si_2O_7 \cdot {}^1/_4MX$ (MX = NaCl (**I**), NaBr (**II**), KCl (**III**), KBr (**IV**)) with an open framework structure of chromous disilicate hosting alkali-metal halides.

Experimental Section

In experiments aiming for the synthesis of chromous silicates using alkali-metal halides as flux we observed the title compounds for the first time. While we never have obtained Cr_2SiO_4,[11] the disilicates $Cr_3Si_2O_7 \cdot {}^1/_4MX$ (MX: NaCl, NaBr, KCl, KBr) could be synthesized from mixtures of Cr_2O_3 (Merck), Cr (Johnson Matthey Chemicals), SiO_2 (Serva), and NaCl, NaBr, KCl, or KBr (Merck) according to eq 1. The

$$Cr(s) + Cr_2O_3(s) + 2SiO_2(s) + {}^1/_4MX(l) \rightarrow Cr_3Si_2O_7 \cdot {}^1/_4MX(s) \quad (1)$$

MX: NaCl, NaBr, KCl, KBr

starting materials were used without further purification. In a typical experiment aproximately 0.9 mmol of Cr_2O_3, 1.2 mmol of Cr, 2 mmol of SiO_2, and 0.5−1 mmol of alkali-metal halide were mixed thoroughly and cold-pressed (20−30 kN) into pellets.

Reactions were carried out in evacuated silica tubes ($\phi \sim 8.5$ mm, thickness of walls ∼ 4 mm) at ∼1620 K (measured by thermocouples PtRh 30%/PtRh 6%) for 2 days. After being cooled to room temperature (rate: 200°/h) the silica tubes were white and brittle from recrystallization. Even though the temperatures employed were above the softening point of quartz, the tubes were still sealed. We assume that the saturation pressure of the flux stabilized the ampules. Yet in some experiments the tubes did show leaks after heating. In those cases the reaction product was dark green with no indication for Cr^{II}. On account of higher costs and more difficult handling, we prefer the described use of silica tubes to platinum tubes. Intensely purple samples of small bunched crystals of the title compounds were obtained besides incompletely reacted educts. The amount of byproducts could be reduced using a small surplus of Cr and additional alkali-metal halide, which could be washed off with water after the reaction. The elemental compositions of $Cr_3Si_2O_7 \cdot {}^1/_4KCl$ and $Cr_3Si_2O_7 \cdot {}^1/_4KBr$ were checked by X-ray fluorescence spectroscopy. Within the limits of the method they are in agreement with the results of structure determination. Well-shaped single crystals were grown as thin square plates with edge lengths up to 1 mm by employing 1 mmol alkali-metal halide and the reactants as thoroughly mixed powders instead of pellets. The color of the plates is light purple because of the thinness of the crystals. $Cr_3Si_2O_7 \cdot {}^1/_4NaBr$ is a little more reddish, and $Cr_3Si_2O_7 \cdot {}^1/_4KCl$ more blueish. Growth patterns appear as squares on the surface of the plates. At ambient temperatures in air **I**−**IV** are stable against oxidation. They dissolve slowly in dilute HF. Experiments with CsI, CsCl, RbCl, KI, NaI, LiCl, and TlCl were carried out under similar conditions but did not lead to the formation of any chromous compounds.

Magnetic measurements on powdered samples of selected crystals of **I**−**IV** were carried out on a Faraday balance in the temperature range

† E-mail: robert.glaum@anorg.chemie.uni-giessen.de.

⊗ Abstract published in *Advance ACS Abstracts,* September 15, 1997.

(1) Part of planned Ph.D. thesis of A.S., Justus-Liebig-University Giessen, 1997.
(2) Glaum, R.; Özalp, D.; Walter-Peter, M.; Gruehn, R. *Z. Anorg. Allg. Chem.* **1991**, *601*, 145.
(3) Gerk, M. Ph.D. Thesis, Justus-Liebig-University Giessen, 1996.
(4) Glaum, R.; Schmidt, A. *Z. Anorg. Allg. Chem.* **1997**, in press.
(5) Glaum, R. *Z. Kristallogr*. **1992**, *205*, 69.
(6) Glaum, R. *Z. Anorg. Allg. Chem.* **1992**, *616*, 46.
(7) Monnier, A.; Berset, G.; Schmid, H.; Yvon, K. *Acta Crystallogr*. **1987,** *C43*, 1243.
(8) Nelmes, R. J.; Thornley, F. R. *J. Phys. C: Solid State Phys*. **1974**, *7*, 3855.
(9) Yoshida, M.; Yvon, K.; Kubel, F. *Acta Crystallogr*. **1992**, *B48*, 30.
(10) Belsky, H. L.; Rossman, G. R.; Prewitt, C. T.; Gasparik, T. *Am. Mineral.* **1984**, *69*, 771.
(11) Dollase, W. A.; Seiffert, F.; O'Neill, H. St. C. *Phys. Chem. Miner.* **1994**, *21*, 104.
(12) Schmidt, A.; Glaum, R.; Beck, J. *J. Solid State Chem.* **1996**, *127*, 331.

S0020-1669(97)00071-2 CCC: $14.00

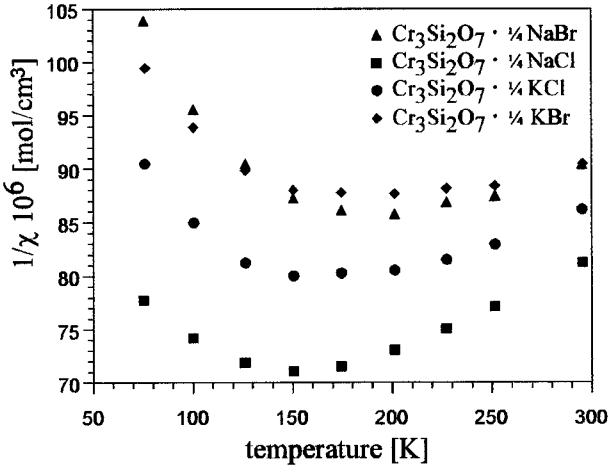

Figure 1. $1/\chi_m$ vs temperature for powders from selected crystals of **I**−**IV**.

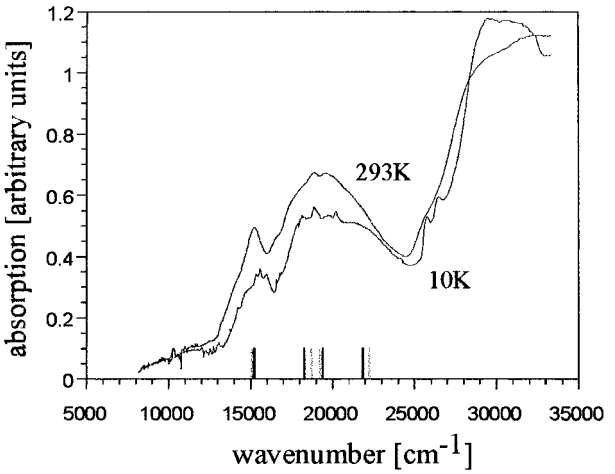

Figure 2. Absorption spectra of $Cr_3Si_2O_7 \cdot {}^1/_4NaBr$ at 10 and 293 K (two different samples): d−d transitions at 15 500, 19 000, and 21 500 cm^{-1}. Ticks at the bottom indicate transition energies for Cr1 (black) and Cr2 (gray) calculated within the framework of the angular overlap model.

from 295 to 76 K (Figure 1). The curves of the reciprocal molar susceptibilities versus temperature show broad minima in the range 150 K (chlorides) to 210 K (bromides), indicating fairly strong low-dimensional antiferromagnetic coupling of the Cr^{II}. The absorption spectrum of $Cr_3Si_2O_7 \cdot {}^1/_4NaBr$ (Figure 2) has been recorded at 10 and 293 K (two different samples) on a suspension of powdered crystals in poly(dimethylsiloxane) mulling agent held between quartz disks. For the measurements a Cary-17 spectrophotometer has been used with a Janis Research Super Vari-Temp cryogenic dewar mounted in the optical path. The spectrum shows a broad band around 19 000 cm^{-1} with a shoulder at 21 500 cm^{-1} and a weaker band around 15 500 cm^{-1}.

Structure Determination and Description

X-ray Investigations. Single-crystal data for **I**−**IV** were collected on an AED-2 four-circle diffractometer (Siemens). The structures were determined applying direct methods (SHELXS-86)[13] and refined with the program SHELXL-93.[14] Details on the structural investigations and crystallographic data for the four compounds are summarized in Table 1. An empirical absorption correction employing ψ-scans[15] was applied to all

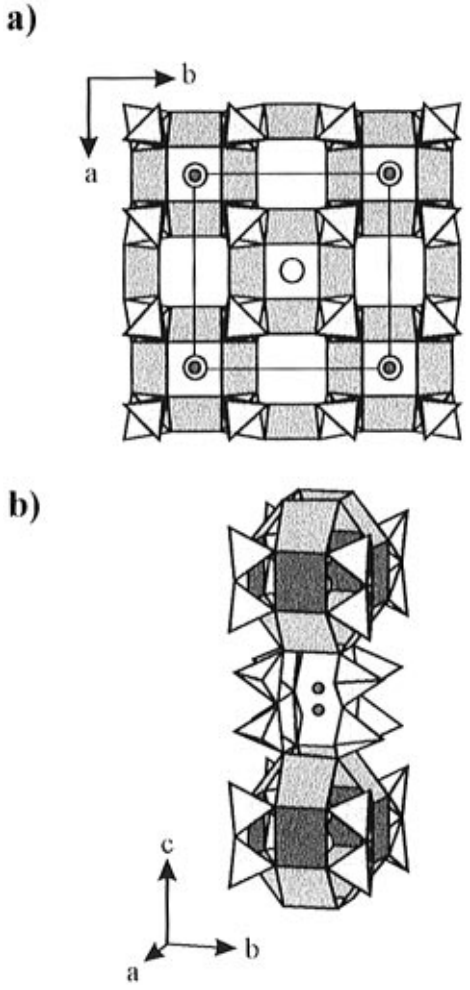

Figure 3. ATOMS[35] representation of the $Cr_3Si_2O_7 \cdot {}^1/_4MX$ structure type: (a) Projection of the structure on the *ab*-plane; (b) perspective drawing with emphasis on the two cage types. Key: [$Cr1O_4$], dark gray, [$Cr2O_4$], grey; [Si_2O_7], light gray; M^+, small circles; X^-, large circles.

data sets. Table 2 presents the final atomic coordinates and isotropic displacement parameters U_{eq}. Anisotropic refinement of M and X in the two special positions (2a) 0, 0, 0 (M) and (2b) 0, 0, $^1/_2$ (X) led to comparatively high *R*-values, large atomic displacement parameters in the *z*-direction for M and X, and maxima of about 7 $e^-/Å^3$ close to the sites in Δ-Fourier syntheses. We then tried refinement of M and X on half-occupied split positions (4e) 0, 0, *z*, with isotropic displacement parameters. Δ-Fourier syntheses still revealed residual electron density (∼5 $e^-/Å^3$) left in between the split positions. In the final refinements we therefore allowed split positions as well as anisotropic displacement parameters for M and X. This led to slightly enlarged displacement parameters for M and X in the *z*-direction with residual electron densities of less than 2 $e^-/Å^3$ and acceptable conventional residuals between $0.02 \leq R \leq 0.08$. Allowing free refinement of the site occupation factor of M and X led to no significant deviation from ideal occupancy. Thus, only a narrow homogenity range with respect to the alkali-metal halide content of the chromous disilicate framework can be expected. We assume that the occupation of the positions "above" and "below" the mirror plane in *I4/mmm* is statistical. No hints for a superstructure or incommensurate lattices could be found from precession and Weissenberg photographs. Despite these photographs being in perfect agreement with the high-symmetrical Laue-group 4/*mmm* we tried refinement of the structures by assuming the lower-symmetrical space groups *I*4*mm* and *I*422. Even so the disorder in the structure could

(13) Sheldrick, G. M. SHELXS-86: Program for Crystal Structure Solution, Univ. Göttingen, 1986.
(14) Sheldrick, G. M. SHELXL-93: Program for Crystal Structure Refinement, Univ. Göttingen, 1993.
(15) North, A. C. T.; Phillips, D. C.; Mathews, F. S. *Acta Crystallogr.* **1968**, *A24*, 351.

Table 1. Experimental X-ray Diffraction Parameters and Crystal Data for $Cr_3(Si_2O_7) \cdot {}^1/_4MX$

	chem formula			
	$Cr_3(Si_2O_7) \cdot {}^1/_4NaCl$ (**I**)	$Cr_3(Si_2O_7) \cdot {}^1/_4NaBr$ (**II**)	$Cr_3(Si_2O_7) \cdot {}^1/_4KCl$ (**III**)	$Cr_3(Si_2O_7) \cdot {}^1/_4KBr$ (**IV**)
a (Å)[a]	10.254(2)	10.2596(7)	10.385(1)	10.391(1)
c (Å)[a]	12.960(4)	12.969(3)	12.975(2)	12.967(4)
cell vol (Å^3)	1362.7(6)	1365.1(3)	1399.3(3)	1400.1(5)
formula units	$Z = 8$	$Z = 8$	$Z = 8$	$Z = 8$
fw	338.79	349.91	342.82	353.93
space group	*I*4/*mmm* (No. 139)	*I*4/*mmm*	*I*4/*mmm*	*I*4/*mmm*
temp (K)	293	293	293	293
λ (Mo Kα) (Å)	0.710 73	0.710 73	0.710 73	0.710 73
ρ_{calc} (g/cm^3)	3.303	3.405	3.254	3.358
abs coeff (mm^{-1})	$\mu = 5.158$	$\mu = 6.515$	$\mu = 5.156$	$\mu = 6.485$
R1[b]	0.0827	0.0247	0.0375	0.0670
wR2[c]	0.0749	0.0551	0.0755	0.0858

[a] From single crystal data (four-circle diffractometer). [b] $R1 = \sum(|F_o - F_c|)/\sum|F_o|$. [c] $wR2 = \sum[w(F_o^2 - F_c^2)]/\sum[w(F_o^2)^2]^{1/2}$.

Table 2. Postional Parameters and Equivalent Isotropic Displacement Values (Å^2)[a] for **I**−**IV** with Estimated Standard Deviations in Parentheses

	x	y	z	U_{eq}
		$Cr_3(Si_2O_7) \cdot {}^1/_4NaCl$ (**I**)		
Na	0	0	0.041(1)	0.036(4)
Cl	0	0	0.4398(7)	0.037(2)
Cr1	0.3255(1)	0	$^1/_2$	0.0105(3)
Cr2	0.22885(9)	0	0.28558(6)	0.0083(2)
Si	0.2172(1)	0.2172(1)	0.1116(1)	0.0061(3)
O1	0.1631(4)	0.1631(4)	0	0.006(1)
O2	0.1422(2)	0.1422(2)	0.2030(3)	0.0073(7)
O3	0.3129(3)	0.1278(3)	0.3832(2)	0.0094(6)
		$Cr_3(Si_2O_7) \cdot {}^1/_4NaBr$ (**II**)		
Na	0	0	0.0388(7)	0.035(2)
Br	0	0	0.4757(2)	0.0365(8)
Cr1	0.32576(8)	0	$^1/_2$	0.0096(2)
Cr2	0.22948(5)	0	0.28555(4)	0.0082(2)
Si	0.21704(5)	0.21704(5)	0.11165(6)	0.0054(2)
O1	0.1627(2)	0.1627(2)	0	0.0081(6)
O2	0.1422(2)	0.1422(2)	0.2035(2)	0.0072(4)
O3	0.3139(2)	0.1279(2)	0.3829(1)	0.0101(3)
		$Cr_3(Si_2O_7) \cdot {}^1/_4KCl$ (**III**)		
K	0	0	-0.0423(4)	0.0210(7)
Cl	0	0	0.4320(5)	0.035(1)
Cr1	0.31898(9)	0	1/2	0.0092(2)
Cr2	0.22727(6)	0	0.28298(4)	0.0079(1)
Si	0.22141(6)	0.22141(6)	0.11236(6)	0.0052(2)
O1	0.1706(2)	0.1706(2)	0	0.0066(5)
O2	0.1443(2)	0.1443(2)	0.2014(2)	0.0071(4)
O3	0.3089(2)	0.1254(2)	0.3817(1)	0.0095(3)
		$Cr_3(Si_2O_7) \cdot {}^1/_4KBr$ (**IV**)		
K	0	0	0.0399(6)	0.021(1)
Br	0	0	0.4739(4)	0.037(2)
Cr1	0.3183(2)	0	$^1/_2$	0.0085(3)
Cr2	0.2278(1)	0	0.28266(7)	0.0074(3)
Si	0.2215(1)	0.2215(1)	0.1126(1)	0.0046(3)
O1	0.1710(4)	0.1710(4)	0	0.006(1)
O2	0.1440(3)	0.1440(3)	0.2014(3)	0.0056(8)
O3	0.3093(3)	0.1256(3)	0.3813(2)	0.0086(6)

[a] $Ueq = {}^1/_3\sum_i\sum_j U_{ij}a_i^*a_j^*a_ia_j$.

not be resolved. No satisfying result with large correlation matrix elements, nonpositive definite displacement parameters, and still remaining high values of residual electron densities were obtained. Selected bond lengths and angles from the final refinements of **I**−**IV** are listed in Table 3.

Structure Description. Two crystallographically independent chromium atoms in **I**−**IV** are in almost square-planar coordination (d(Cr−O) ∼ 2.02 Å) with the chromium atoms being slightly (∼0.1 Å) out of plane (Table 3 and Figure 4). Three of these [CrO_4] squares centered by Cr2, Cr1 and Cr2 are connected by sharing O3−O3 edges. Thus, bent [$Cr_3O_4O_{4/2}$] units are formed with d(Cr1−Cr2) ∼ 2.96 Å. The dihedral angle between the best-fit planes through [$Cr1O_4$] and [$Cr2O_4$] is ∼143° (Figure 4). In the [$Cr2O_4$] unit three angles ∠(O,Cr1,O) ∼ 93° and one ∠(O,Cr1,O) ∼ 81° are observed, with the small angle between the O3 atoms of the common edge. Consequently, for [$Cr1O_4$] being in the center of the trimer two small angles ∠(O,Cr1,O) ∼ 82° and two larger ∠(O,Cr1,O) ∼ 98°

Table 3. Selected Interatomic Distances (Å) and Angles (deg) for $Cr_3(Si_2O_7) \cdot {}^1/_4MX$ (MX = NaCl, NaBr, KCl, KBr) with Estimated Standard Deviations in Parentheses

	$Cr_3Si_2O_7$			
	$^1/_4$NaCl	$^1/_4$NaBr	$^1/_4$KCl	$^1/_4$Br
Cr1−O3^{1,8,9} (4×)	2.006(3)	2.011(2)	2.016(2)	2.020(3)
Cr2−O3^8 (2×)	2.015(3)	2.016(2)	2.014(2)	2.014(3)
Cr2−O2^6 (2×)	2.015(2)	2.015(1)	2.027(1)	2.026(2)
Si−O2	1.608(4)	1.612(2)	1.618(2)	1.619(4)
Si−O3^{12}	1.620(3)	1.624(2)	1.624(2)	1.623(3)
Si−O3^7	1.620(3)	1.624(2)	1.624(2)	1.623(3)
Si−O1	1.646(3)	1.648(2)	1.638(2)	1.638(3)
∠(Si,O1,Si)	123.1(3)	122.9(2)	125.8(2)	126.1(4)
M−O1^{10,11,3} (4×)	2.425(6)	2.414(4)	2.565(4)	2.566(6)
M−O2^{6,3,5} (4×)	2.94(1)	2.970(7)	2.958(4)	2.978(7)
X−Cr1^{4,3,2} (4×)	3.427(3)	3.357(1)	3.428(2)	3.325(2)
X−Cr2^{3,6,5} (4×)	3.082(6)	3.409(2)	3.051(5)	3.428(3)
[O_4]−Cr1[a]	0.129(3)	0.122(2)	0.105(2)	0.094(4)
[O_4]−Cr2[a]	−0.069(2)	−0.072(1)	−0.071(1)	−0.076(3)
φ[b]	143.15(7)	142.86(4)	143.85(5)	143.64(8)
Cr1−Cr2	2.950(1)	2.951(1)	2.972(1)	2.971(1)

[a] Distance of Cr1 and Cr2, respectively, from the best-fit planes through the four ligands. [b] Dihedral angle between the best-fit planes through [$Cr1O_4$] and [$Cr2O_4$]. Symmetry codes: (1) $x, y, -z + 1$; (2) $-x, -y, -z + 1$; (3) $-y, x, z$; (4) $y, -x, -z + 1$; (5) $-x, -y, z$; (6) $y, -x, z$; (7) $-x + {}^1/_2, -y + {}^1/_2, -z + {}^1/_2$; (8) $x, -y, z$ (9) $x, -y, -z + 1$; (10) $-x, -y, -z$; (11) $y, -x, -z$; (12) $-y + {}^1/_2, -x + {}^1/_2, -z + {}^1/_2$.

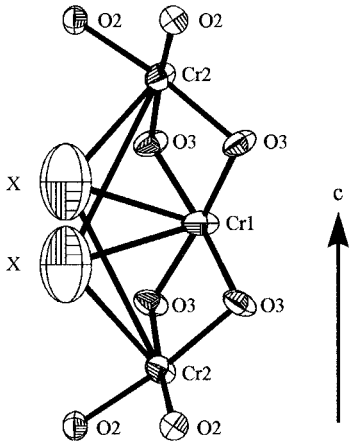

Figure 4. ORTEP[34] view of a trimer [$Cr_3O_4O_{4/2}$] with adjacent split position for X^-. Ellipsoids (for $Cr_3Si_2O_7 \cdot {}^1/_4NaCl$) are given with 97% probability. The atom-labeling scheme is the same as in Table 3.

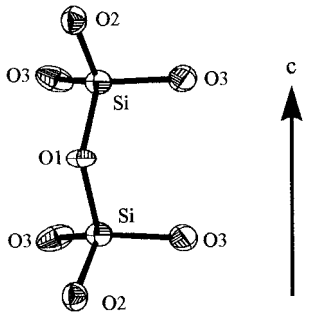

Figure 5. ORTEP[34] view of a disilicate group in $Cr_3Si_2O_7 \cdot {}^1/_4NaCl$. Ellipsoids are given with 97% probability. The atom-labeling scheme is the same as in Table 3.

are observed. Four of these trimers, related by the four-fold axis, are connected through the corners of the remaining two oxygen atoms O2 of the top and bottom $Cr2O_4$ squares. In the resulting hollow $[Cr_{12}O_{24}]$ unit a halide ion is located slightly off-center on the half-occupied Wyckoff position (4e), 0, 0, *z*, instead of (2b), 0, 0, $^1/_2$ (Figures 3 and 4). It is worth noting that the displacement away from the special position (2b) is significantly larger for chlorine than for bromine [*z*(Cl) ∼ 0.436; *z*(Br) ∼ 0.475]. Thus, Cl^- is surrounded by only eight Cr^{II} (4 × Cr2 at ∼3.07 Å, 4 × Cr1 at ∼3.40 Å) with an effective coordination number ECoN[16−18] of ∼7.2, while there are 12 Cr^{II} contributing to the coordination of Br^- (4 × Cr1 at ∼3.33 Å, 4 × Cr2 at ∼3.42 Å, and 4 × Cr2 at ∼3.92 Å) with ECoN(Br^-) ∼ 10.4. For the calculation of effective coordination numbers the program MAPLE-4[19] has been used. The $[SiO_4]$ tetrahedra of the disilicate group are almost regular with an average bond length *d*(Si−O) ∼ 1.63 Å. A rather small bridging angle ∠(Si,O,Si) ∼ 125° with eclipsed conformation of the disilicate group (Figure 5) is observed. Disilicate groups connect individual $[Cr_{12}O_{24}]$ units to a three-dimensional network (Figure 3). Thus, the "backbones" of four $[Si_2O_7]$ form a second type of cage hosting, again slightly off-center, the alkali-metal cations M^+ on the half-occupied site (4e), 0, 0, *z* (*z* ≈ 0.04), instead of (2a), 0, 0, 0. M is surrounded by eight oxygen atoms (4 × O1 at ∼2.5 Å, 4 × O2 at ∼2.95 Å) with an effective coordination number ECoN[16−18] of ∼5.2 calculated for Na^+ and ∼6.5 for K^+. Therefore, an effective coordination number ECoN(O1) ∼ 2.9 for the bridging oxygen O1 in the disilicate group is obtained. It is remarkable that there are additional empty channels in the $Cr_3Si_2O_7$ framework extending along [$^1/_2$, 0, *z*] and [0, $^1/_2$, *z*] besides the filled voids piled along [0, 0, *z*] and [$^1/_2$, $^1/_2$, *z*] (Figure 3a).

Discussion

The structure type can be described as an expanded NaCl structure ($a_{\text{"NaCl"}} = a_{Cr_3Si_2O_7 \cdot 1/4MX} + b_{Cr_3Si_2O_7 \cdot 1/4MX}$) with an intergrown $[Cr_3Si_2O_7]$ framework. It is another example besides [BaCl][$CuPO_4$][20] for an unusual cage structure built from square-planar $[M^{II}O_4]$ and tetrahedral units like $[Si_2O_7]$ or $[PO_4]$. The cages of the chromous disilicate framework can only accommodate Na^+ and K^+ as cations and Cl^- and Br^- as anions, although one would expect from consideration of ionic radii that other monovalent ions might fit as well. The size of the voids can be estimated from the distance between two Cr1 atoms on opposite faces of a $[Cr_{12}O_{24}]$ cage. Approximately 6.68 Å for the sodium-containing compounds and ∼6.62 Å for the potassium compounds are observed. Some information about the energetic situation of the positions within the cages is gained from calculation of the Coulomb potential *U* (using computer program MAPLE-4[19]) along [0, 0, *z*] omitting M and X. The curve $U = f(z)$ is given in Figure 6, showing a wide maximum for $0.35 \le z \le 0.65$ (position of X^-) and a minimum for $-0.10 \le z \le 0.10$ (position of M^+). We take the broad minima and maxima in the potential curve, which are similar to those observed in ionic conductors, as an explanation for the observed indistinct positions of M and X. Similar calculations of the Coulomb potential were carried out for the empty channel along [$^1/_2$, 0, *z*] (Figure 6). The minima in this curve (possible site for M^+) are far less pronounced than those found along [0, 0, *z*] where the cages are actually occupied by M^+. Although the Coulomb potential at [$^1/_2$, 0, 0] and [$^1/_2$, 0, $^1/_2$] is as positive as the one at [0, 0, $^1/_2$], the former positions show no chemically reasonable coordination for a halide anion. We assume that these are the reasons for the strict preferance of M^+ and X^- for their experimentally observed positions.

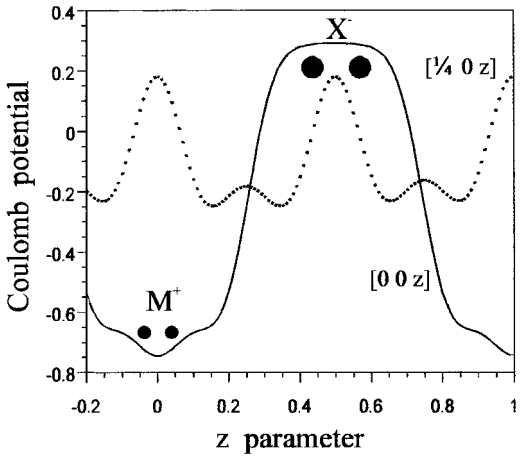

Figure 6. Coulomb potential vs site parameter *z* along [0, 0, *z*] (solid line) and [$^1/_2$, 0, *z*] (dotted line) in $Cr_3Si_2O_7 \cdot {}^1/_4NaCl$. Small circles indicate the actually occupied split positions for M^+, and large circles are for X^- along [0, 0, *z*].

With the accurate structural information available for the four isotypic compounds $Cr_3Si_2O_7 \cdot {}^1/_4MX$ (MX = NaCl, NaBr, KCl, and KBr) detailed examination of influences of M and X on the structure type becomes possible. The volume of the unit cell increases significantly from the sodium compounds to those containing potassium, while variation of the halide has no effect. The larger unit cell volume is completely due to an increase of the crystallographic *a*-axis. The *c*-axis is unaffected by any variation of the interstitial ions M^+ and X^-. This behavior can be understood by comparing bridging angles ∠(Si,O1,Si) and distances M−O1. While *d*(K−O1) is much longer (∼2.57 Å) than *d*(Na−O1) (∼2.42 Å), the distances M−O2 are not significantly longer for M = K. The increased *d*(K−O1) is accompanied by larger Si,O1,Si bridging angles for the potassium compounds (∠∼126°) than for those containing sodium (∠∼123°). The bridging angle Si,O1,Si is ∼125° with eclipsed conformation of the disilicate group (Figure 5). Even though being very small, the ∠(Si,O1,Si) of ∼125° is not unusual. For the bridging oxygen ECoN(O1) ∼ 2.9 is calculated. According to Gibbs[21] the bond angle for three-coordinated oxygen in $[Si_2O_7]$ groups ranges between about 124 and 137°. The relatively long $Si-O_{br}$ bond is correlated to a small Si,O,Si angle. The square-planar coordination of the Cr^{II} with a mean

(16) Hoppe, R. *Angew. Chem., Int. Ed. Engl.* **1966**, *5*, 95.
(17) Hoppe, R. *Z. Kristallogr.* **1979**, *150*, 23.
(18) Hoppe, R. *Z. Naturforsch.* **1995**, *50a*, 555.
(19) Hübenthal, R. MAPLE-4: Program for calculating the madelung part of lattice energy. Justus-Liebig-University Giessen, Germany, 1993.
(20) Etheredge, K. M. S.; Hwu, S.-J. *Inorg. Chem.* **1995**, *34*, 3123.
(21) Gibbs, G. V. *Am. Mineral.* **1982**, *67*, 421 (cited in Liebau, F. *Structural Chemistry of Silicates*; Springer Verlag: Berlin, 1985).

distance d(Cr−O) ∼ 2.02 Å is comparable to d(Cr−O) = 2.000 Å found for the [$Cr^{II}O_4$] in $CaCrSi_4O_{10}$[10]. For Cr^{II} with additional ligands above and below the basal plane generally longer equatorial bond lengths d(Cr−O) ∼ 2.05 Å [12] are observed. One might attribute the slightly longer bond length d(Cr−O) in the $Cr_3Si_2O_7{\cdot}^1/_4MX$ (MX = NaCl, NaBr, KCl, and KBr) compared to $CaCrSi_4O_{10}$ to weak axial bonding interaction of the Cr^{II} with the halide ions. While Cr^{II} in plain square-planar coordination ($CaCrSi_4O_{10}$) is red, chromous compounds in a more regular octahedral environment are blue to turquoise ($CrSO_4{\cdot}5H_2O$,[22] $Cr_2P_2O_7$,[2,3] $Cr_3[B_7O_{13}]X$[1,23]). In that sense the purple color of $Cr_3Si_2O_7{\cdot}^1/_4MX$ (MX = NaCl, NaBr, KCl, and KBr) might be taken as indication for a small but significant influence of the axial halide ligands. However, the distances d(Cr−X) found here [3.08, 3.43, and 4.26 Å for X = Cl; 3.36, 3.41, and 3.89 Å for X = Br] are much longer than the ones observed in $CrCl_2$ (d(Cr−Cl): 4 × 2.39, 2 × 2.90 Å)[24] and $CrBr_2$ (d(Cr−Br): 4 × 2.55, 2 × 3.00 Å).[25]

Calculations on the d-orbital energies of Cr^{II} were performed within the framework of the angular overlap model (AOM),[26] using the computer program CAMMAG.[27] With parameters B = 664 cm^{-1}, C = 2712 cm^{-1}, ζ = 184 cm^{-1} (each 80% of the free ion[28]), e_σ(Cr−O) = 7600 cm^{-1}, $e_{\pi,x}$(Cr−O) = $e_{\pi,y}$(Cr−O) = $^1/_4e_\sigma$(Cr−O), and e_{ds} = 1750 cm^{-1} the observed transitions could be matched nicely (cf. Figure 2). The parameters employed here correspond to those used for chromous oxo compounds like $CrSO_4{\cdot}5H_2O$[22] and α-$Cr_2P_2O_7$.[29] They also permit modeling of the polarized spectra observed for $CaCrSi_4O_{10}$.[10] The unusually high ds-mixing parameter[30] e_{ds} accounts for the degression of the 3d(z^2) orbital by configuration interaction with the 4s orbital. A total stabilization of the 3$d(z^2)$ orbital of about 5500 cm^{-1} by this effect is in agreement with an orbital sequence d($x^2 - y^2$) >> d(xy) > d(xz, yz) > d(z^2) for Cr^{II} in square-planar coordination. For $CaMSi_4O_{10}$ (M^{II} = Cr,[10,33] Fe,[31] Cu[32]) this orbital sequence is experimentally well established and explained along the lines only summarized here. Our calculations do not allow an accurate estimation of the influence of the axial halide ions on the energy of the Cr^{II} d-orbitals because it is impossible to distinguish between the effects of e_{ds} and weak σ-bonding of the axial ligands. However, e_σ(Cr-Br) in $Cr_3Si_2O_7{\cdot}^1/_4NaBr$ should not exceed 500 cm^{-1}.

Although we have observed rather strong low-dimensional antiferromagnetic coupling (Figure 1) for $Cr_3Si_2O_7{\cdot}^1/_4MX$ (MX = NaCl, NaBr, KCl, and KBr), the mean distance d(Cr1−Cr2) ∼ 2.96 Å appears too long for direct magnetic exchange. As the magnetic structure of α-$Cr_2P_2O_7$[33] shows, antiferromagnetic coupling occurs among Cr^{II} connected via two oxygen bridges (edge-sharing polyhedra). Thus, complete antiferromagnetic ordering within the [$Cr_{12}O_{24}$] cages without magnetic long-range ordering appears possible. The presence of three-dimensional magnetic ordering will be checked by neutron diffraction experiments, which are planned.

Acknowledgment. We thank Mr. G. Koch for the collection of the X-ray data and Miss V. Krausch for her dedicated assistance in the synthetic work. A.S. is grateful for having had the possibility to collect some of the results presented here at Stanford University. Many thanks to Prof. Ed Solomon and his group for their hospitality during a stay made possible by financial support through a DAAD scholarship (HSPII/AUFE).

Supporting Information Available: A full table of experimental X-ray and crystal data (2 pages). Four X-ray crystallographic files, in CIF format, are available. Ordering and access information is given on any current masthead page.

IC9700718

(22) Hitchman, M. A.; Lichon, M.; McDonald, R. G.; Smith, P. W.; Stranger, R.; Skelton, B. W.; White, A. H. *J. Chem. Soc., Dalton Trans.* **1987**, 1817.
(23) Nesterova, N. N.; Pisarev, R. V.; Andreeva, G. T. *Phys. Stat. Sol.* **1974**, *65b*, 103.
(24) Tracy, J. W.; Gregory, N. W.; Lingafelter, E. C. *Acta Crystallogr.* **1962**, *15*, 672.
(25) Tracy, J. W.; Gregory, N. W.; Lingafelter, E. C.; Dunitz, J. D.; Mez, H.-C.; Rundle, R. E.; Scheringer, C.; Yakel, H. L.; Wilkinson, M. K. *Acta Crystallogr.* **1961**, *14*, 927.
(26) Jørgensen, C. K. *Modern Aspects of Ligand Field Theory*, North Holland, Amsterdam, 1970; and references therein. Schäffer, C. E. *Struct. Bonding (Berlin)* **1968**, *5*, 68.
(27) Gerloch, M. *Magnetism and Ligand-Field Analysis*, Cambridge University Press: Cambridge, U.K., 1983. Gerloch, M.; McMeeking, R. F. *J. Chem. Soc., Dalton Trans.* **1975**, 2443.
(28) Figgis, B. N. *Introduction to Ligand Fields*; Krieger Publishing Co.: Malabar, FL, 1986.
(29) Glaum, R. Unpublished results, 1995.
(30) Smith, D. W. *Inorg. Chim. Acta* **1977**, *22*, 107.
(31) Mackey, D. J.; McMeeking, R. F.; Hitchman, M. A. *J. Chem. Soc., Dalton Trans.* **1979**, 299.
(32) Ford, R.; Hitchman, M. A. *Inorg. Chim. Acta* **1979**, *33*, L167.
(33) Glaum, R.; Stüsser, N. *Experimental Reports, Berlin Neutron Scattering Center;* Hahn-Meitner-Institute: Berlin, 1996; p 93.
(34) Johnson, C. K. *ORTEP-II;* Report ORNL-5138; Oak Ridge National Laboratory: Oak Ridge, TN, 1976.
(35) Dowty, E. *ATOMS for Windows, Vers.3.1; Shape Software*: 521 Hidden Valley Road, Kingsport, TN 37663, **1994**.